Joint Communication and Sensing Using Compressive Sensing and a Single Multi-Mode Multi-Port Antenna

NILS L. JOHANNSEN [1], JAN MIETZNER[2] (Senior Member, IEEE), AND PETER A. HOEHER [1] (Fellow, IEEE)

[1]Chair of Information and Coding Theory, Kiel University, 24143 Kiel, Germany

[2]Department of Media Technology, University of Applied Sciences Hamburg, 22081 Hamburg, Germany

CORRESPONDING AUTHOR: N. L. JOHANNSEN (e-mail: nj@tf.uni-kiel.de)

ABSTRACT Joint communication and sensing (JCAS) is of special interest due to densification in various contexts like wireless networks, airspace, and transportation networks. In this paper, a JCAS approach using a single multi-mode multi-port antenna (M^3PA) element is proposed. Towards this goal, circular beamforming is applied in order to separate communication and sensing channels, using the unique capabilities of M^3PA s. The sensing possibilities using only a single M^3PA element are evaluated assuming compressive sensing and MIMO radar signal processing including the polarization domain. Simulation results for an unmanned aerial vehicle scenario indicate a good separation of the communication link and sensing system at the cost of a slightly increased angular error.

INDEX TERMS Beamforming, compressive sensing, joint communication and sensing, multi-mode multi-port antennas.

I. INTRODUCTION

JOINT communication and sensing (JCAS) is of increasing interest due to the densification of smart devices in a multitude of applications, such as autonomous flights and the Internet of Things (IoT), and is therefore also of interest for the development of sixth-generation (6G) mobile networks [1]. Towards the goal of increased spectral efficiency as well as reduced hardware effort due to shared resources, different approaches apply. Orthogonal transmission schemes are of most interest, typically based on orthogonal frequency-division multiplexing (OFDM) or, due to its smaller peak to average power ratio, orthogonal time-frequency space (OTFS) signaling [2], [3], [4]. Comprehensive literature surveys are given in [1], [5], [6], [7]. In particular, for unmanned aerial vehicles (UAVs) that are the focus of our numerical results, weight constraints are an important consideration. As discussed, e.g., in [7], line-of-sight (LOS) propagation between the UAVs is desirable due to high required data rates when operating as a

swarm. Depending on the application, UAV s are expected to operate in stand-alone scenarios, like packet delivery or public transport, or as a part of a larger swarm, e.g., for surveillance or search and rescue, as well as mapping on the one hand and delivering communication links to users on the other hand [6]. Especially in the latter context, the payload and space onboard of each individual UAV are strongly limited.

To overcome this issue, multi-mode multi-port antennas (MMMPAs, M^3PA s) provide a promising solution: they offer multiple ports and therefore pattern diversity at a reduced installation space [8], [9]. In [10], [11], a square-shaped M^3PA providing six ports has been proposed, based on the theory of characteristic modes. The theory of characteristic modes has been used as well in [12] to also design a square-shaped antenna. This one has a perimeter of about four wavelengths, allowing nearfield communication and sensing. In this regard, a constant field intensity is desired, which is opposed to the requirements of sensing using beamforming.

In [13], an array consisting of a different type of M^{3}PA s has been constructed: each element of the array provides two antenna ports, designed to allow beamforming, but not providing the opportunity to steer the polarization. The steering of polarization would directly be allowed by the antenna proposed in [14], which also requires an antenna array to allow beamforming. A summary, characterization, and analysis of different possible types of single-element beamforming, especially for M^{3}PA s, is provided in [15]. In recent works, M^{3}PA s have been proven to be suitable for communication [16] as well as for direction-of-arrival (DoA) estimation [17], [18].

In recent years, compressive sensing (CS) has been investigated for several different tasks and goals. In [19], a scenario for an airborne application of CS has been discussed. There, it is shown that CS provides good results compared to classical beamforming approaches. In [20], the sparsity of the signal domain due to the sparsity of the environment is exploited by CS to jointly perform communication and sensing assuming a mobile network scenario, serving several users. Other works focus on the establishment of joint beamforming and trajectory optimization to allow JCAS, as in [21], [22]. Some of these allow simultaneous communication and sensing based on different beams in conjunction with CS [23]. However, both [19] as well as [21] focus on the applicability of a particular CS algorithm and an alternative optimization setup to an antenna array with isotropic antenna elements, respectively. While in [19] the communication aspect is not foreseen and instead an optimized array geometry is searched, in [21] the trajectory flown by the UAV is also included. In [23], an array structure employing the antenna positions only is taken into account, also optimizing the trajectory of a scan.

Motivated by this prior art, in this paper the objectives of wireless communication using M^{3}PA s on one hand and sensing on the other hand are merged and the pattern diversity provided by the M^{3}PA s proposed in [10] is exploited

- to enable LOS circular polarization-based communication links,
- to separate the communication channel from the sensing channel using polarization diversity, and
- to perform CS as an example for a low complexity detection algorithm based on a single antenna element.

In particular, the capabilities of the M^{3}PA allow to save resources in time and frequency domain using just a single antenna element: by applying polarization for parallel communication and sensing, the signals do not have to be separated in different frequency bands or time slots. To illustrate this feature, an example of a transmission scheme making use of the different signal processing approaches presented in this paper is given. Focus is on the sensing capabilities using the patterns of the antenna from [10], [11], while allowing an additional communication link, using a CS algorithm for the sensing part and just a single M^{3}PA element, which is described by its manifold matrix.

The paper is organized as follows: in Section II, the underlying system model for the sensing (radar) and wireless communication part is discussed, including an example protocol for combining sensing and communication and a detailed description of the M^{3}PA. In Section III, the considered beamforming, radar processing, and CS algorithms are described. Numerical sensing and communication performance results are presented in Section IV, and conclusions are drawn in Section V.

II. SYSTEM MODEL

In this paper, a single user participating in a network of UAV s is under investigation. The UAV shall be able to perform joint sensing based on a radar signal and wireless communication based on a beamforming codebook, which shall allow the UAV to be seen as a part of a JCAS system. Let us assume a UAV performing sensing in a first iteration step. During sensing, targets are separated by their range-Doppler cell, which can be determined by well-known techniques [24], [25].

In Fig. 1(a), a UAV sensing its neighbor is illustrated. In the context of this paper, range-Doppler processing is assumed as a first step of the sensing. The second sensing step provides an estimate of the azimuth and elevation angles, which are delivered by applying CS. The sensing waves are pictured as black circles, originated from the antenna of the UAV under consideration. The antenna aboard is drawn as a square, while the considered UAV is highlighted by the black color. In regard of a successful application of CS, a sparse solution space is required. Sparsity is given if nearly all entries in the signal domain under determination are equal to zero. As motivated in [19], it is unlikely that more than one airborne target can be found in the same range-Doppler cell. This is due to the fact that other targets would have to travel with exactly the same relative velocity and distance to the UAV under consideration. In the context of this work, it is assumed that the CS algorithm is only applied for those range-Doppler cells which deliver a target detection. However, in the presence of simultaneous wideband communication, any range-Doppler cell will be disturbed.

To avoid interference, the UAV under consideration is assumed to establish a communication link to its neighboring device, by utilizing the polarization diversity offered by the M^{3}PA. In Fig. 1(b), a right-hand circular polarized (RHCP) communication link is indicated by two red arrows: the first one for transmission and the second one for reception. Since both UAV s know their positions relative to each other (because prior sensing is assumed to be successfully completed), they are able to employ codebook-based beamforming for both transmission and reception, creating the RHCP-based communication link. A two-way communication link could be established by adding a conventional duplexing mechanism, such as time division duplex (TDD), frequency division duplex (FDD), or code division duplex (CDD).
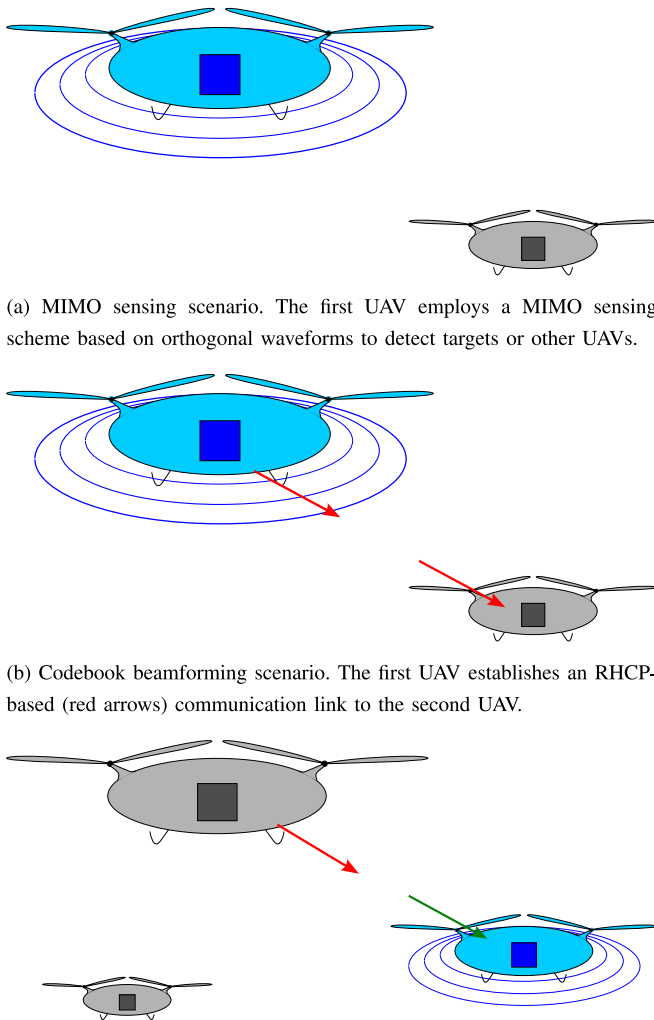
(a) MIMO sensing scenario. The first UAV employs a MIMO sensing scheme based on orthogonal waveforms to detect targets or other UAVs.

(b) Codebook beamforming scenario. The first UAV establishes an RHCP-based (red arrows) communication link to the second UAV.

(c) Communication link suppression scenario. The receiving UAV can employ a suppression of the communication link while performing own sensing, e.g. of another UAV. If beamforming is done digitally, simultaneous reception of both the radar and the communication link is possible.

FIGURE 1. Illustrations of different scenarios. Each UAV is assumed to carry at least one M³PA, depicted as a square aboard. The blue UAV is the one under investigation of the different scenarios. Blue circles indicate sensing, red and green arrows RHCP and LHCP polarization at transmitter and receiver, respectively.

The receiver can distinguish between the communication and the radar response of a target by applying different polarizations. On the one hand, a common polarization of the desired communication signal and the receiver allows the reception of the communication link. On the other hand, the communication link can be seen as undesired interference to the radar signal. Thus, employing the opposite polarization for sensing in the direction of the transmitter suppresses this interference. As a result, the receiver is capable of receiving a radar response of a radar target. This scenario is depicted in Fig. 1(c). As above, the red arrow indicates the RHCP component at the transmitter. Meanwhile, the receiver allows simultaneous left-hand circular polarized (LHCP) reception (green arrow) at this pair of angles only, which enables
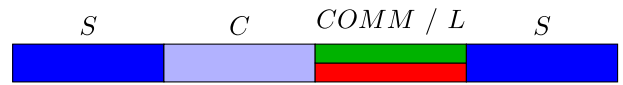

FIGURE 2. Example protocol allowing communication as well as sensing. Modes used in the scheme include a *search mode (S)*, a *confirmation mode (C)*, a *communication mode (COMM)*, and a *listen mode (L)*.

sensing (blue circles) of a possible third target (smaller gray UAV).

These different situations in the scenario under consideration require different approaches for sensing: given the first situation prior establishing the connection, multiple-input multiple-output (MIMO) radar processing using orthogonal signaling across the multiple antenna ports is promising. Once the communication link is established, polarization shall be applied by beamforming. To illustrate these ideas more clearly – and to highlight the special benefits offered by the M³PA s in this context – we will consider a corresponding example protocol for accommodating the sensing and wireless communication operations.

A. EXAMPLE PROTOCOL FOR SENSING AND COMMUNICATION

The different scenarios mentioned above have different requirements. To successfully apply both sensing and communication, an example protocol is shown in Fig. 2. Starting with the *sensing mode (S)*, mainly two scenarios are applicable. If no a priori knowledge about other UAV s is given, an omni-directional sensing employing orthogonal signals as discussed in Fig. 1(a) can be used. If the directions of other UAV s are known a priori, their sensing signals can be suppressed analogously to Fig. 1(c). Alternatively, the provided time slot for mode S could be partitioned between multiple UAV s by applying a suitable carrier-sense/collision avoidance protocol.

The second time slot is dedicated to a *confirmation mode (C)*, during which the positions of targets detected during mode S are verified by applying codebook beamforming (described in detail in Section III). Here, a codebook maximizing the gain in the direction of each target focuses the signal power in the desired directions, leading to an increased signal-to-noise ratio (SNR). If a codebook is applied, which allows only one polarization in the direction to the target, then mode C could be used in parallel to the *communication mode (COMM)*. The *communication mode (COMM)* – depicted here in a separate time slot – enables the transmission of data via a particular polarization (e.g., RHCP, red) between two UAV s, analogously to Fig. 1(b). Alternatively, the receiving UAV could suppress the communication link, (e.g., via LHCP polarization, green), applying the orthogonal polarization at the particular angle, and may then use the time slot for another sensing phase (along the lines of Fig. 1(c)). Given a perfect match of angles as well as ideal hardware, parallel sensing at the receiver is thus possible. Limits of the proposed scheme arise from misalignment of the beam, which leads

to a reduced suppression capability. Further, hardware limits arise from a large required dynamic range obeying linearity, which allows the simultaneous reception and processing of a radar echo as well as a (potentially much stronger) communication link. In contrast, the beamforming based on a pseudo-inverse can be calculated efficiently for small numbers of ports, which is fulfilled for M^3PA s. However, for the successful integration of further links, as well as the reception of transmitted data, an additional *listen mode (L)* needs to be included. During the listening mode, the listening UAV receives transmitted data by applying the correct polarization towards the direction of the transmitting UAV. Additionally, it can distinguish this link from another UAV trying to join the communication, provided that the existing link and the setup of a new link is also separated by different polarizations: the new UAV, which would like to join the traffic, could use an LHCP wave in the direction of its communication target. The target can apply both polarizations to distinguish between the already existing link (e.g., RHCP) and the new one (e.g., LHCP). Once the connection is established, polarization should be changed from the initialization polarization (e.g., LHCP) to the polarization nominally used for communication. As discussed, new UAV s trying to connect can be detected by their occurrence in several range-Doppler cells.

After the time slot for the mode *COMM/L* is finished, the protocol continues with the next time slot for mode *S*.

B. DESCRIPTION OF THE M^3PA

Let the UAV be equipped with the square-shaped M^3PA proposed in [11]. This antenna provides six ports on a single radiator. Each antenna port corresponds to an antenna pattern

$$f_p(\vartheta, \varphi) = \begin{bmatrix} F_{\theta,p}(\vartheta, \varphi) \\ F_{\phi,p}(\vartheta, \varphi) \end{bmatrix}, \tag{1}$$

where $F_{\theta,p}(\vartheta, \varphi)$ and $F_{\phi,p}(\vartheta, \varphi)$ denote the antenna fields of antenna port p in the linear polarization along θ and ϕ at the pair of angles (ϑ, φ), respectively. As described in [10], these antenna patterns excited by port p and q of the M^3PA are mutually orthogonal in the far field, i.e., the envelope correlation coefficient (ECC) vanishes:

$$C_{\mathrm{ECC}} = \frac{\oint_{\Omega} |f_p(\vartheta, \varphi)^H \cdot f_q(\vartheta, \varphi)|^2 d\Omega}{\oint_{\Omega} |f_p(\vartheta, \varphi)|^2 d\Omega \cdot \oint_{\Omega} |f_q(\vartheta, \varphi)|^2 d\Omega} = 0 \tag{2}$$

$\forall\, p \neq q$, where $(.)^*$ denotes complex conjugate. The solid angle $\Omega(\vartheta, \varphi)$ is defined as a surface element of the sphere. This orthogonality and independent ports shall be exploited to allow sensing based on a single antenna element. The number of ports is denoted as $N_{\mathrm{p,Tx}}$ and $N_{\mathrm{p,Rx}}$ if operated as a transmit or receive antenna, respectively.

To evaluate the concept of the M^3PA for a communication and sensing application, perfectly matched and lossless ports are assumed, each having the same efficiency of 100%. As a result, the antenna gain pattern of each port needs to be normalized as

$$\frac{4\pi}{2Z_0} \oint_{\Omega} |F_{\theta,p}(\vartheta, \varphi)|^2 + |F_{\phi,p}(\vartheta, \varphi)|^2 d\Omega \stackrel{!}{=} 1, \tag{3}$$

where Z_0 is the impedance in free space.

C. DEFINITION OF THE RADAR CHANNEL
For the description of the channel model, let the field response of the transmit antenna port p be given by $f_{\mathrm{Tx},p}(\vartheta, \varphi)$ as in (1). The transmitted waves are assumed to propagate from the antenna towards a reflecting surface. The reflection can be described by applying the Jones calculus for electromagnetic waves. Since the same antenna is assumed to be employed for both transmission and reception, the fields received at port p can be described by the fields transmitted at the same port:

$$f_{\mathrm{Rx},p}(\vartheta, \varphi) = f_{\mathrm{Tx},p}^*(\vartheta, \varphi). \tag{4}$$

Hence, the radar signal $s_{\mathrm{RAD},r,t}$ received at receive (Rx) antenna port r given the transmission of a signal at transmit (Tx) antenna port t and reflected at the pair of angles ϑ and φ is described by the antenna fields in transmit and receive direction according to

$$s_{\mathrm{RAD},r,t} = \frac{4\pi}{2Z_0} f_{\mathrm{Rx},r}(\vartheta, \varphi)^T \boldsymbol{J} f_{\mathrm{Tx},t}(\vartheta, \varphi)$$
$$\sqrt{\kappa(d)} e^{-j\psi(d)} s_{\mathrm{SEN},t} \sqrt{P_{\mathrm{RAD,Tx},t}}, \tag{5}$$

where $\kappa(d)$ describes the attenuation, $\psi(d)$ the phase shift of the signal corresponding to the distance d between antenna and target, and $s_{\mathrm{SEN},t}$ the transmit sensing signal at port t with power $P_{\mathrm{RAD,Tx},t}$. The Jones matrix $\boldsymbol{J}$ describes the reflection at the target:

$$\boldsymbol{J} = \begin{bmatrix} j_{11} & j_{12} \\ j_{21} & j_{22} \end{bmatrix} = \begin{cases} \begin{bmatrix} 1 & 0 \\ 0 & -1 \end{bmatrix} & \text{if reflected} \\ \begin{bmatrix} 0 & 0 \\ 0 & 0 \end{bmatrix} & \text{if not.} \end{cases} \tag{6}$$

The attenuation is given by

$$\kappa(d) = \frac{\lambda^2 \sigma}{(4\pi)^3 d^4}, \tag{7}$$

where λ is the wavelength of the considered signal and σ corresponds to the radar cross section (RCS) of the target. Throughout this paper, an attenuation $\kappa(d) = 1$ is assumed without loss of generality, which allows regulating the SNR by adjusting the noise power. The definition of the SNR is discussed in Section II-E. The phase term can be written as

$$\psi(d) = 2\pi \frac{\lambda}{d}. \tag{8}$$

Subsequently, the phase term $\psi(d)$ is modeled by a uniformly distributed random process, $\mathcal{U}[0, 2\pi)$.

The received radar signal

$$s_{\mathrm{RAD}} = \begin{bmatrix} s_{\mathrm{RAD},1}^T, \dots, s_{\mathrm{RAD},N_{\mathrm{p,Tx}}}^T \end{bmatrix}^T$$

with $s_{\text{RAD},t} = [s_{\text{RAD},1,t}, \ldots, s_{\text{RAD},N_{\text{p,Rx}},t}]^T$ is assumed to provide unit power as

$$\mathbb{E}\left\{\sum_t s_{\text{RAD},t}^H s_{\text{RAD},t}\right\} = \mathbb{E}\{s_{\text{RAD}}^H s_{\text{RAD}}\} = 1. \quad (9)$$

The transmit index t describes the number of orthogonal transmissions, which is $N_{\text{p,Tx}}$ if a MIMO scheme is employed and 1, if transmit beamforming without orthogonal signaling is applied.

D. DEFINITION OF THE COMMUNICATION SIGNAL

Throughout this paper, the communication link is described by the incident signal impinging from the angles ϑ_C, φ_C of the LOS path to the signal source. Since an RHCP link is given, the field vector of the impinging wave is defined as $f_{\text{imp}} = 1/\sqrt{2}[1, -j]^T$. Analogously to the impinging wave at the radar receiver, the normalized received communication signal can be written as

$$s_{\text{COM},r,t} = \sqrt{\frac{4\pi}{2Z_0}}f_{\text{Rx},r}(\vartheta_C, \varphi_C)^T f_{\text{imp}} s_{\text{COM,Tx},t}\sqrt{P_{\text{COM,Tx}}}, \quad (10)$$

where the index term t denotes the diversity regime employed at the radar transmitter. E.g., if a multi-carrier scheme is used, the antenna responses to the communication signals of the different frequencies need to be taken into account. The quasi-random phase $\psi(d)$ of the radar signal leads to uncorrelated phases between communication and radar signals. The power of the communication signal is defined as

$$\mathbb{E}\left\{\sum_t s_{\text{COM,Tx},t}^H s_{\text{COM,Tx},t}\right\} = \rho. \quad (11)$$

Hence, the signal to interference power ratio between the radar signal and the interfering communication signal is $1/\rho$.

E. DEFINITION OF THE SNR

Let the received signal at port r originated from port t be denoted by

$$y_{r,t} = s_{\text{RAD},r,t} + s_{\text{COM},r,t} + n_{r,t}, \quad (12)$$

where $n_{r,t}$ is an additive white Gaussian noise (AWGN) term with zero mean and variance $\sigma_{\text{n},r,t}^2$. To calculate the SNR of the radar system, the received signal power of the radar signal is defined as

$$P_{\text{RAD,Rx},r} = \mathbb{E}\left\{\sum_t |s_{\text{RAD},r,t}|^2\right\} = \sum_{t=1}^{N_{\text{Tx}}} P_{\text{RAD,Tx},t}, \quad (13)$$

which is valid if the antenna patterns are mutually orthogonal. If the transmit power for each antenna port is chosen such that $\sum_t P_{\text{RAD,Tx},t} = P_{\text{RAD,Tx}} = 1$, the SNR at each receiver can be set by defining $\mathbb{E}\{|n_r|^2\} = \sigma_{\text{n},r,t}^2 = 1/\text{SNR}$.

F. DEFINITION OF THE CHANNEL CAPACITY

Since the received signal response of the radar system is not known to the communication link in advance, it is treated as an unknown interference term to the communication link. The capacity of the communication link normalized with respect to the bandwidth of the communication link then is calculated as

$$C = \log_2(1 + \text{SINR}_{\text{COM}}) = \log_2\left(1 + \frac{\rho}{1 + \sigma_{\text{n},r,t}^2}\right), \quad (14)$$

where the signal-to-interference-plus-noise ratio of the communication link is denoted as SINR_{COM}. The variance $\sigma_{\text{n},r,t}^2$ corresponds to the SNR of the radar system, as defined in Section II-E.

III. BEAMFORMING AND RADAR PROCESSING

For the description of the radar signal processing by CS, the definition of a sensing matrix is mandatory. This contains possible beamforming vectors as well as the radiation field characteristics of the given antenna structure, namely the manifold matrix [26] of the transmitting as well as receiving M^3PA. The radar aspect of the received signal vector as well as the CS problem then is described by

$$s_{\text{RAD}} = Ax, \quad (15)$$

where $A \in \mathbb{C}^{N_{\text{p,max}} \times N_{\text{Angles}}}$ is the sensing matrix with $N_{\text{p,max}} = N_{\text{p,Tx}}N_{\text{p,Rx}}$ and x is the target vector of length N_{Angles} defining the possible angles of the radar target. Each row of A contains the combinations of the antenna response vectors from (5) for each angle. Throughout, we employ a uniform grid in the angular domain to set up the sensing matrix A.

A. MIMO RADAR

Column a_i of the sensing matrix A is described based on the field vectors

- Rx antenna response in θ-polarization $f_{\theta,\text{Rx},i}$,
- Rx antenna response in ϕ-polarization $f_{\phi,\text{Rx},i}$,
- Tx antenna response in θ-polarization $f_{\theta,\text{Tx},i}$, and
- Tx antenna response in ϕ-polarization $f_{\phi,\text{Tx},i}$.

If a MIMO radar is assumed, and the transmitted radar signals at the transmit ports are mutually orthogonal, by either choosing a time division, code division, or frequency division scheme, the sensing matrix is calculated by

$$a_{\text{MIMO},i} = \frac{4\pi}{2Z_0}\left[j_{11}f_{\theta,\text{Rx},i} \otimes f_{\theta,\text{Tx},i} + j_{22}f_{\phi,\text{Rx},i} \otimes f_{\phi,\text{Tx},i}\right]^T. \quad (16)$$

Here, the Kronecker product $\otimes$ achieves a port-wise multiplication of the field patterns and yields a $1 \times N_{\text{p,max}}$ sensing vector. This vector corresponds to the system response a target given at this particular angle at index i would generate. The Jones matrix from (6) is represented by the coefficients j_{11} and j_{22}. Note that the MIMO radar mode operates with a mixed polarization, employing linear polarization both along θ and ϕ.

B. BEAMFORMING

A similar description can be used for cases in which beamforming is applied. If beamforming is applied at the transmitter, no orthogonal signals have to be used. Instead, the transmit antenna patterns are used to form a beam and therefore reduce the degrees of freedom of the radar system by lowering the length of the sensing vector to either $N_{\mathrm{p,Tx}}$, if a receive beamforming is applied, or $N_{\mathrm{p,Rx}}$, if a transmit beamforming is used. The sensing vector given transmit beamforming is then written as

$$a_{\mathrm{Tx},i} = \frac{4\pi}{2Z_0}\Big[j_{11}f_{\theta,\mathrm{Rx},i}\big(f_{\theta,\mathrm{Tx},i}^T w_{\mathrm{Tx}}\big) \\ + j_{22}f_{\phi,\mathrm{Rx},i}\big(f_{\phi,\mathrm{Tx},i}^T w_{\mathrm{Tx}}\big)\Big]^T. \tag{17}$$

In the case of transmit beamforming (one signal is sent via a single precoding vector), the received signal vector required in order to apply CS is achieved by the diversity at the receiver. Vice versa, if reception beamforming shall be applied, a MIMO signal needs to be transmitted, such that still a suitable sensing matrix can be established and used for calculation by the CS algorithm. Hence, each signal allows the adaptation of an individual beamforming vector. This leads to the introduction of a receive beamforming matrix W_{Rx}. This matrix W_{Rx} provides $N_{\mathrm{p,Tx}}$ beamforming vectors, each of which can be optimized to the corresponding transmit pattern. Since the orthogonality allows separation of the signals of the different transmitters at the receiver, the sensing vector is taken from the elements of the principal diagonal:

$$a_{\mathrm{Rx},i} = \frac{4\pi}{2Z_0}\Big[j_{11}\ \mathrm{diag}\big((W_{\mathrm{Rx}}^T f_{\theta,\mathrm{Rx},i})f_{\theta,\mathrm{Tx},i}\big) \\ + j_{22}\ \mathrm{diag}\big((W_{\mathrm{Rx}}^T f_{\phi,\mathrm{Rx},i})f_{\phi,\mathrm{Tx},i}\big)\Big]^T. \tag{18}$$

Subsequently, two different beamforming options applicable via a corresponding codebook at the transmitter are discussed:

- maximizing the gain in a desired direction and
- achieving a desired polarization.

Finally, the calculation of a beamforming matrix at the receiver is discussed, allowing the suppression of a known communication link based on circular polarization. In each scenario in which a beamforming vector is applied, the sensing matrix reduces to $A \in \mathbb{C}^{N_{\mathrm{p,red}} \times N_{\mathrm{Angles}}}$, where

$$N_{\mathrm{p,red}} = \begin{cases} N_{\mathrm{p,Rx}}, & \text{if a transmit beamforming is applied, or} \\ N_{\mathrm{p,Tx}}, & \text{if a receive beamforming is applied} \end{cases} \tag{19}$$

is the reduced number of ports, dependent on the application of either transmit or receive beamforming. For the evaluation of the beamforming, the achieved channel gains as a function of the angle are of interest. These can be calculated by

$$G_{\mathrm{Chan}} = \Big(\frac{4\pi}{2Z_0}\Big)^2\big[w_{\mathrm{Rx}}^T F_{\mathrm{Rx},i}^T J F_{\mathrm{Tx},i} w_{\mathrm{Tx}}\big]^2, \tag{20}$$

where the field matrices $F_{\mathrm{Rx},i}$ and $F_{\mathrm{Tx},i}$ are described by the field responses at the angle with index i:

$$F = \begin{bmatrix} F_{\phi,1} & \dots & F_{\phi,N_{\mathrm{p}}} \\ F_{\theta,1} & \dots & F_{\theta,N_{\mathrm{p}}} \end{bmatrix}, \tag{21}$$

where N_{p} denotes the number of angles within the employed uniform angular grid.

1) MAXIMIZING THE GAIN

If the transmitted power in direction of a certain angle of departure shall be maximized, the antenna gain in the desired direction needs to be maximized. The antenna gain can be calculated by

$$G(\varphi, \vartheta) = \frac{4\pi}{2Z_{\mathrm{F}}}\Big[\Big|\sum_p w_p F_{\phi,p}(\varphi, \vartheta)\Big|^2 + \Big|\sum_p w_p F_{\theta,p}(\varphi, \vartheta)\Big|^2\Big], \tag{22}$$

where w_p corresponds to the precoding coefficient of the p-th port and $F_{\theta,p}(\varphi, \vartheta)$ and $F_{\phi,p}(\varphi, \vartheta)$ describe the electric field coefficients in θ and ϕ polarization for departure angles φ and ϑ. This equation can be rewritten using the matrix notation according to (21) as [27]

$$G = |Fw|^2. \tag{23}$$

Thus, the optimization problem can be formulated as follows:

$$\text{maximize}_w\ \{G(\varphi, \vartheta)\} = \text{minimize}_w\{ -|Fw|^2\}, \\ \text{subject to}\quad |w|^2 \leq 1. \tag{24}$$

For the optimization of the gain, this non-convex optimization problem is reformulated as

$$\text{maximize}\ w^H F^H Fw, \tag{25}$$

where FF^H is positive semi definite. Applying Lagrange multipliers, the optimization problem is reformulated as

$$\text{maximize}\ \mathcal{L}(w, \lambda) = \text{maximize}\ w^H F^H Fw - \lambda\big(w^H w - 1\big). \tag{26}$$

To find the maximum of the function, the derivative

$$\frac{\partial \mathcal{L}}{\partial w} = 0 = Fw - \lambda w \tag{27}$$

yields the well-known Eigenvalue problem. Hence, the solution of the problem is the Eigenvector v belonging to the largest eigenvalue $\lambda_{\max}$

$$w = v_{\lambda_{\max}} \in \mathrm{col}(V), \tag{28}$$

where V is the matrix of Eigenvectors and col(.) denotes the corresponding set of column vectors. Note that the gain maximization is jointly performed for both polarizations θ and ϕ.

2) CIRCULAR POLARIZATION

Along with the number of orthogonal ports of an M^{3}PA allowed on a certain antenna structure, different portions of polarizations at each angle can be addressed. Each port refers to a specific combination of polarizations, either given by vertically and horizontally polarized components or given by RHCP waves and LHCP waves. Under the assumption of the field components given by f_θ and f_ϕ, the field responses to a circular wave can be formulated as

$$f_R = f_\theta - jf_\phi \qquad (29)$$
$$f_L = f_\theta + jf_\phi. \qquad (30)$$

At a given angle, one component (e.g., LHCP, f_L) shall be suppressed, while the other (e.g., RHCP, f_R, correspondingly) shall be maintained or ideally be maximized. This beamforming option would, for example, serve the scenario in Fig. 1(b), where the first UAV wants to establish an RHCP-based communication link in the direction of the second UAV. Accordingly, the LHCP component of the antenna pattern needs to be suppressed in this direction. We propose to apply a least squares solution to find an optimized precoding vector for the selection of the polarizations according to

$$\text{minimize}_{w_{R/L}} \quad \left\{ |F_{R,L}w_{R/L} - \chi_{R/L}|^2 \right\},$$
$$\text{subject to: } |w_{R/L}|_2^2 = 1, \qquad (31)$$

where $|.|_2$ denotes $L2$-norm,

$$F_{R,L} = \begin{bmatrix} F_{R,1} & \dots & F_{R,P} \\ F_{L,1} & \dots & F_{L,P} \end{bmatrix}, \qquad (32)$$

and the polarization selection vector is defined as $\chi_L = [0,1]^T$ or $\chi_R = [1,0]^T$. The indices R (RHCP) and L (LHCP) denote the type of polarization. Since suppression of a polarization requires that both the real and imaginary parts of the component are zero, the phase can be adjusted as desired. Any phase angles can be achieved by applying a phase shift to the resulting precoding vector. After calculating the vector w_{LS} by least-squares, the constraint is applied by

$$w = \frac{w_{LS}}{|w_{LS}|_2}. \qquad (33)$$

The gain of the resulting polarization given the field pattern matrix $F_{R,L}$ can be calculated according to (23).

3) RECEPTION BEAMFORMING

If a communication link has been established, this receive beamforming option would, for example, serve the scenario in Fig. 1(c), where the second UAV decides to utilize the current time slot for sensing rather than for receiving the communication signal. To this end, a beamforming solution is required, which maximizes the gain in the direction of the target and suppresses the polarization of the transmitting UAV in the corresponding direction. This allows simultaneous sensing of a weaker radar response compared to the interference of the communication link.

From these assumptions, an optimization problem arises: for each beamforming vector at the receiver, the received signal power at the target angle shall be maximized, while suppressing the previously established communication link. In case of parallel digital signal processing and given a sufficient dynamic range of the analog signal processing chain, reception of both communication signal and radar echo simultaneously is possible. This optimization problem is written as

$$\text{maximize} \quad \left\{ |w_{Rx,p}^T F_{Rx} J f_{Tx,p}|^2 \right\}$$
$$\text{subject to: } w_{Rx,p}^H w_{Rx,p} = 1$$
$$w_{Rx,p}^T f_{Rx,PolCom} = 0 \qquad (34)$$

($p = 1, \dots, N_{p,Rx}$). The p-th vector of the beamforming matrix shall provide a maximum signal power given the radiation pattern at the angle of the radar target. The radiation pattern in the direction of the communication link is described by $f_{Rx,PolCom}$, which is defined from the polarization according to (29) or (30). As in (31), a least-squares solution is employed:

$$\text{minimize}_{w_{Rx,p}} \left\{ \left| \begin{bmatrix} g_{Rx,RadTar} \\ f_{Rx,PolCom} \end{bmatrix} w_{Rx,p} - \begin{bmatrix} 1 \\ 0 \end{bmatrix} \right|^2 \right\}. \qquad (35)$$

The vector of channel coefficients $g_{Rx,RadTar}$ of the radar channel is defined by

$$g_{Rx,RadTar} = F_{Rx} J f_{Tx,p}, \qquad (36)$$

which represents the channel gain. The beamforming vector at the receiver is finalized by

$$w = \frac{w_{Rx,p}}{|w_{Rx,p}|_2}, \qquad (37)$$

which realizes the constraint of a unity gain receiver.

C. SENSING ALGORITHM

To find the correct angular cell, a CS approach is used. To formulate the sensing problem, (15) is approximated as

$$\min_x |Ax - y|_1. \qquad (38)$$

Recall that x is sparse and $|.|_1$ denotes $L1$-norm. The sensing problem (38) is solved by using an orthogonal matching pursuit (OMP) algorithm [19]. The OMP algorithm estimates the column, in which the target most likely is expected. Each column of the sensing matrix A corresponds to a pair of angles in elevation ϑ and azimuth φ. In a first scenario, a MIMO system employing a single M^{3}PA is assumed: orthogonal waveforms are assumed, by either using orthogonality in frequency, time, or code domain. Recall that the sensing matrix of the MIMO scenario consists of $N_{p,max}$ rows.

The MIMO case, which can be seen as an initialization step of the JCAS system, is taken as a reference. However, once the communication link is established, different beamforming scenarios apply. In these scenarios, the sensing

matrix has a reduced size of $N_{\mathrm{p,red}}$ rows, cf. (19). As a straight forward approach, the beamforming weights are calculated offline and stored in the form of a codebook. Each codebook applied to the radar system on one hand reduces the complexity of the OMP algorithm, while limiting the sensing performance due to the smaller number of samples on the other hand.

D. SENSING ERROR

In order to compare the different sensing possibilities, a quality measure for the results is required. Since the sensing matrix represents the antenna field patterns employing spherical coordinates, in this work, we employ the distance defined by the orthodrome as a measure of sensing error. The orthodrome is a well-known measure for the shortest distance of two distinct points located on the surface of a sphere. The distance between these two points can be defined by either a length on the surface of the sphere, or, normalizing to any sphere, by the angle separating both. This angle can be calculated by

$$\cos(\xi) = \sin(\vartheta_1)\sin(\vartheta_2)\cos(\varphi_1 - \varphi_2) + \cos(\vartheta_1)\cos(\vartheta_2), \tag{39}$$

where (ϑ_1, φ_1) and (ϑ_2, φ_2) denote the direction angles of the two points, respectively. A derivation is shown in the Appendix. The sensing error can be averaged for each angle and a number of simulations. Since the M³PA is constructed as a planar radiator above an electrically large ground plane, no radiation/reception can be achieved in the lower hemisphere with regard to the antenna coordinate system. Therefore, to efficiently compare the error in different scenarios (e.g., with different SNR characteristics), the average error on the upper hemisphere is calculated according to

$$\bar{\xi}_{\mathrm{cont}} = \frac{1}{2\pi} \int\limits_{\varphi=0}^{2\pi} \int\limits_{\vartheta=0}^{\pi/2} \xi(\vartheta, \varphi) \sin(\vartheta) d\vartheta\, d\varphi. \tag{40}$$

Since only one hemisphere is taken into account, the normalization coefficient prior the integral is 2π instead of 4π. For the application in a discrete manner, the integrals and averaging coefficients are simplified to

$$\bar{\xi} = \frac{1}{N_\vartheta N_\varphi} \sum_{k=0}^{N_\varphi-1} \sum_{n=0}^{N_\vartheta-1} \xi(\vartheta_n, \varphi_k) \sin(\vartheta_n), \tag{41}$$

where N_ϑ and N_φ denote the number of evaluated angles in azimuth and elevation.

IV. NUMERICAL RESULTS

The following subsections provide some numerical results of CS applied to a single M³PA-element from [11]. This M³PA-element provides six ports and its manifold is sampled with an angular resolution of 5°. As discussed, a MIMO scenario is taken as a reference for the comparison of the codebook-based beamforming. The beamforming performance of each
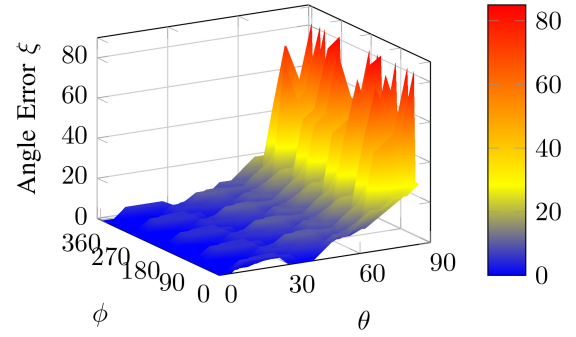
(a) Sensing error. For an angular span of 90° in azimuth and 60° in elevation, errors smaller than 20° occur. The antenna provides a very small estimation error for elevation angles of up to 30°.
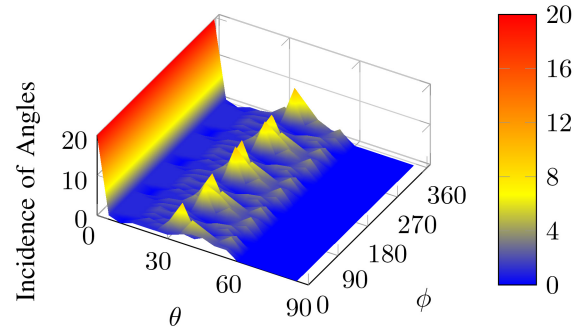
(b) Incidences of estimated angles. The broadside angle at $\vartheta = 0°$ is estimated 22 times, whereas the neighboring angles are not taken into account. An interesting occurance are the periodical maxima along φ at $\vartheta = 35°$. Here, the antenna patterns do not allow a separation by the OMP algorithm.

FIGURE 3. Sensing performance under the assumption of a MIMO radar using orthogonal waveforms given an infinite SNR.

codebook is shown next to the sensing performance. In order to be applicable in a JCAS-scenario, both are of interest. To start with, the sensing performance given the M³PA is tested. Therefore, an infinite SNR as well as the absence of any potential interference by communication links is assumed. Each angle provided in the sensing matrix is tested by setting one target, which results from the assumptions in Section II and [19]. The angles of the target are iterated systematically.

A. SENSING PERFORMANCE IN IDEAL ENVIRONMENT
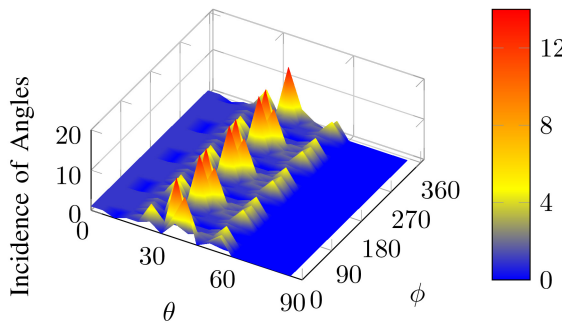#### 1) MIMO SCENARIO (FIG. 3)

This assumption allows to gain an impression of the sensing capabilities of the M³PA under consideration. As can be seen in Fig. 3(a), in the area of the broadside direction ($\vartheta = 0°$, $\varphi = 0°$) of the antenna, rather small errors occur on average. It is noteworthy that the sensing results in a grouping of angles. These groups can be seen as peaks in the histogram in Fig. 3(b). Ideally a flat floor of one entry per angle should be seen in the histogram. This would correspond to the iteration of the target position through all angles. Some estimated angles are selected for a group
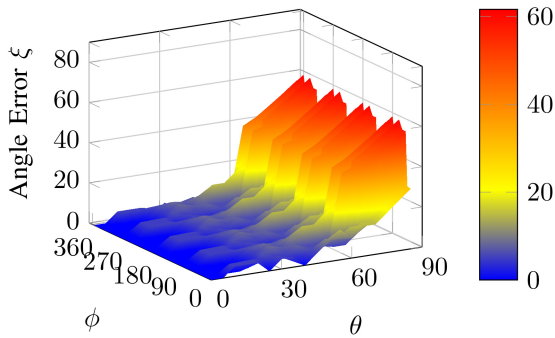
(a) Sensing error. An increased error compared to the MIMO scenario without a beamforming codebook can be noted.
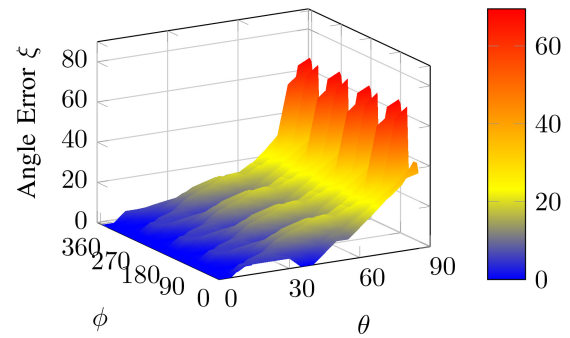
(b) Incidences of estimated angles. The broadside angle at $\vartheta = 0°$ is estimated less often, compared to the MIMO scenario. In the broadside direction, an improvement can be noted. The periodical maxima, are now relocated by 5° along φ at $\vartheta = 40°$.

FIGURE 4. Sensing performance under the assumption of transmit beamforming given an infinite SNR. A codebook maximizing the gain towards a target at a certain angle is assumed.

(a) Sensing error. An increased error compared to the MIMO scenario without a beamforming codebook can be noted.
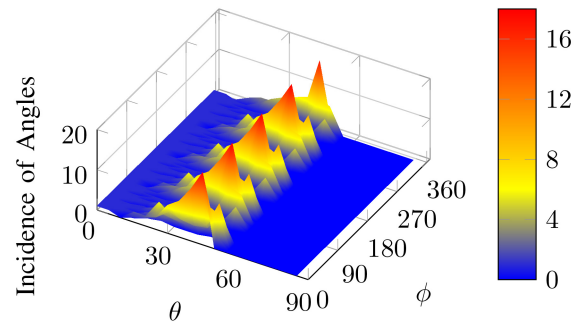
(b) Incidences of estimated angles. The periodical maxima relocated again compared to Fig. 4b along φ towards $\vartheta = 45°$ now. The three largest maxima of each group merged to a single one.

FIGURE 5. Sensing performance under the assumption of transmit beamforming given an infinite SNR. A codebook realizing an RHCP towards a target at a certain angle is assumed.

of incident angles, which can be concluded from the local maxima shown in Fig. 3(b).

2) BEAMFORMING SCENARIO

In the case of beamforming based on a pre- or a decoding vector given by a codebook, in a first step of the evaluation still no interference is assumed. Due to the reduced degrees of freedom and therefore a smaller sensing matrix, a decreased sensing performance is expected.

1) Maximizing the Gain (Fig. 4): If the radiated power in a certain direction is maximized, the corresponding beamforming weights still allow the usage as a radar system. However, as can be seen in Fig. 4(a), compared to the increased signal processing freedom in the MIMO scenario, the performance is reduced, especially for larger angles. In the broadside direction, the maximum vanished and smaller angles are selected more frequently. This can be seen as an improvement in the reduction of sensing errors for some angles, since the algorithm tends to select the broadside angle less frequently. From Fig. 4(b) can be seen that the selected angles occur in groups similar to the ones in Fig. 3(b). The maxima located around $\vartheta = 35°$ in Fig. 3(b) relocate by 5° towards the angle $\vartheta = 40°$.

2) Circular Polarization (Fig. 5): Given a codebook allowing circular beamforming in the direction of the target, for infinite SNRs, the aforementioned groups of selected angles merge. As can be seen in Fig. 5(b), the largest peak now is located at $\vartheta = 45°$. All in all, the error performance of both codebooks is similar. However, the use of circular polarization allows the suppression of a simultaneous communication link. For both codebooks as well as the MIMO approach, elevation angles greater than 60° off broadside direction cannot be detected correctly anymore.

B. SENSING PERFORMANCE IN THE PRESENCE OF NOISE

Throughout each of 50 runs, each entry of the target vector $\boldsymbol{x}$ is iterated and a noise term applied. In these simulations, no interference is assumed. In Fig. 6, the average errors at each angle for each approach are depicted. As can be seen, the increased noise leads to a reduced sensing performance, which is expected. A major impact can be noted at the MIMO radar (Fig. 6(a)), which is due to the fact that beamforming (gain maximization in Fig. 6(b) and circular polarization in Fig. 6(c)) assumes to be focused towards the direction of
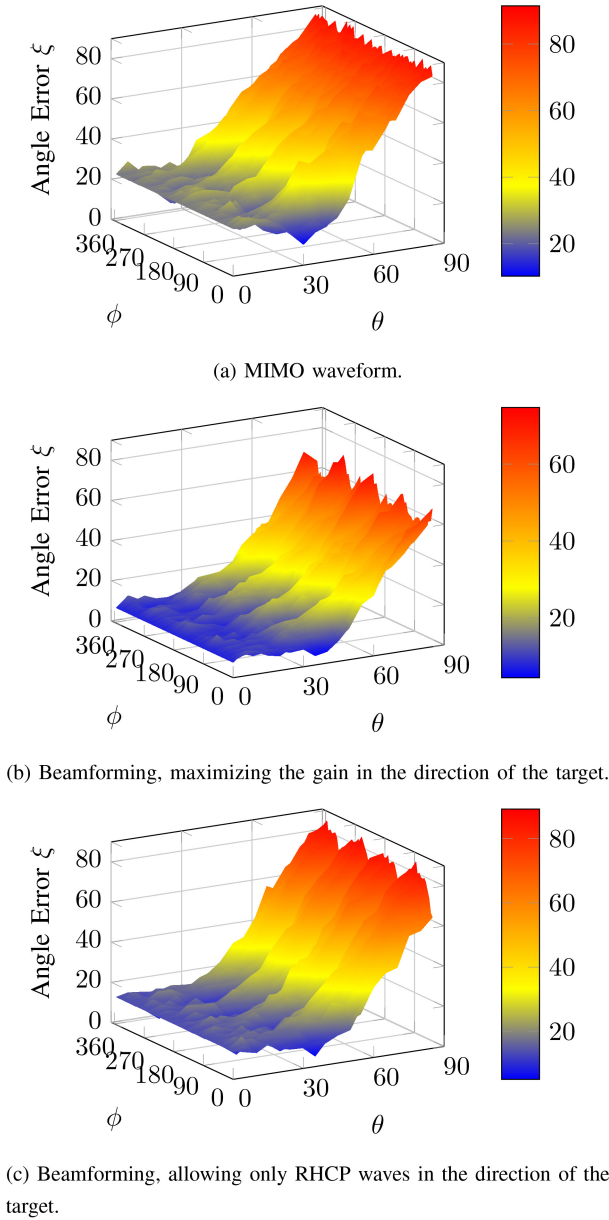
(a) MIMO waveform.

(b) Beamforming, maximizing the gain in the direction of the target.

(c) Beamforming, allowing only RHCP waves in the direction of the target.

FIGURE 6. Sensing performance in the presence of noise. A MIMO radar, employing an M³PA from [11] is assumed. The manifold is sampled with a stepwidth of 5°. A low SNR of −10 dB is assumed to evaluate the capabilities of the antenna. As can be seen, under weak SNR conditions, both beamforming schemes outperform the MIMO approach due to the larger amount of power incident at the target.

FIGURE 7. Average error ξ of the angle estimation as a function of SNR. Different upper limits for the angular domain are taken into account: an angle of 45°, 60°, and 85° from the broadside direction.

advantage, the maximum performance is increased. In the context of a JCAS scenario, transmit beamforming with a circular waveform allows the transmitter of a communication link to sense the presence of the receiver. Alternatively, polarization beamforming allows the receiver, to suppress the interferer and find a possible target in the same direction.

C. SENSING PERFORMANCE WHILE SUPPRESSING INTERFERENCE

Given an established communication link, which might be realized after performing an initial sensing, sensing can be performed at the receiver of the communication link. Using, e.g., an adapted signal power at the transmitter of the communication link prevents the receiver from leaving its dynamic range. As can be seen from Fig. 8(a), a single interferer 20 dB stronger than the radar echo leads to a significant loss in sensing performance. In contrast, the sensing performance for a communication link 30 dB stronger than the radar signal is shown in Fig. 8(b), employing a successful polarization suppression.

The noise power is set to be zero, to find a possible impact of the interference. As can be seen, no negative impact can be seen in the latter case. Recall that throughout this paper, ideal knowledge of radiation patterns and incident angles is assumed. As can be seen, the results of the sensing can be improved, if the radiation pattern can be maximized in the direction of the target online. In summary, the best achievable result employing the M³PA under consideration comes close to the one of the MIMO radar without interfering communication link.

D. COMMUNICATION PERFORMANCE WHILE APPLYING POLARIZATION BEAMFORMING

As discussed in Section IV-C, a communication link with a signal-to-interference ratio up to $\rho = 30\,\text{dB}$ is assumed

the target, which is an advantage compared to the MIMO approach.

In Fig. 7, the average estimation error of the angle is depicted as a function of SNR. The black lines indicate the MIMO signaling waveform, red and blue show a maximization for circular beamforming and gain maximization, respectively. As can be seen, at low SNRs, both beamforming approaches are able to outperform the MIMO sensing waveform. Note that the depicted performances assume an a priori knowledge, such that beamforming towards the target is possible. Due to this
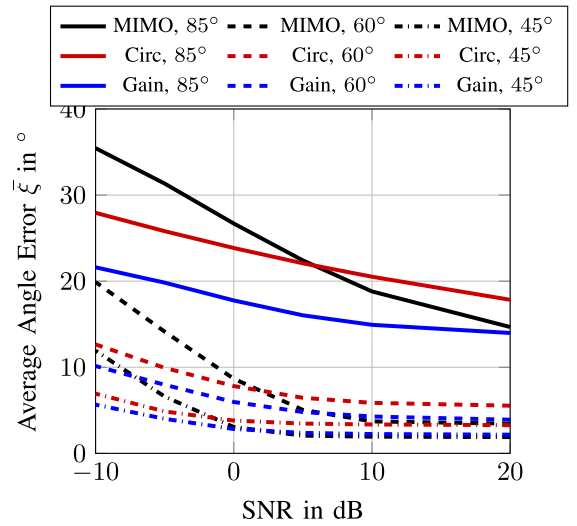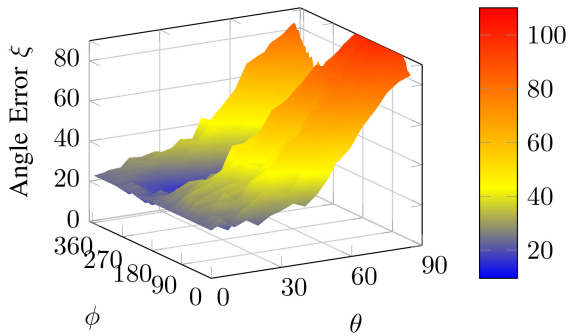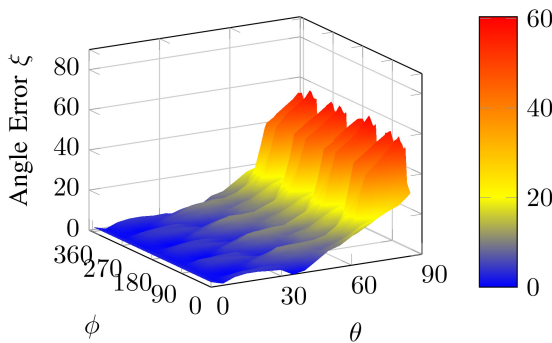
(a) Sensing without suppression of a polarized communication link. An interference power of 20 dB larger than the radar signal is assumed. As can be seen the interfering link has a significant impact on the sensing capabilities.

(b) Sensing with successful suppression of a communication link, using polarization beamforming at the receiver. An infinite SNR as well as an interference power of 30 dB larger than the radar signal is assumed.

FIGURE 8. Ideal sensing performance using a CS algorithm without and with suppression of a communication link, using polarization beamforming. An infinite SNR is assumed in both cases and the results are averaged over 50 runs.

(as described in (11)), where the received radar signal is regarded as the interference in this case. The channel capacity of the corresponding communication link is calculated by applying (14). For each target angle and simulation run, a communication link is set in a random direction. From the point of view of the radar system, this link is seen as an interferer. For each combination and interferer, the channel capacity is calculated and the average across all angles and simulation runs is drawn. The simulation results are shown in Fig. 9. Note that the SNR is defined with regard to the radar signal but not the communication link. In the results, compared to a single-input single-output (SISO) channel, a MIMO / beamforming gain can be noted. E.g., when referring to a SISO channel at the signal-to-interference ratio of $\rho = 30\,\text{dB}$ with no noise present, a capacity $C = \log_2(1001) = 9.96\frac{\text{bps}}{\text{Hz}}$ can be achieved. However, since the M^{3}PA provides 6 ports, the achievable rate increases to $C = \log_2(1 + N_{\text{p,Rx}}\rho) = \log_2(6001) = 12.55\frac{\text{bps}}{\text{Hz}}$.
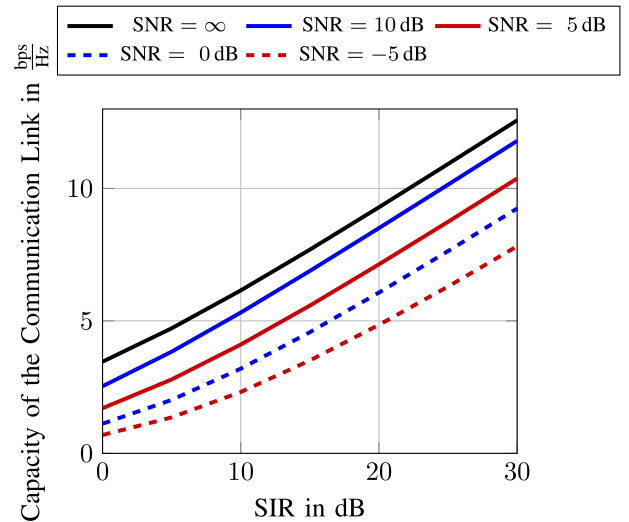

FIGURE 9. Capacity of the communication link, given the signal-to-interference ratio with respect to the radar signal. Note that the provided SNR is defined by the radar signal, as defined in Section II-E and (14).

V. CONCLUSION

In this work, a single M^{3}PA element has been used to enable JCAS based on polarization beamforming. In this context, different scenarios were considered: a MIMO sensing approach using orthogonal waveforms and CS was discussed first. Different codebooks optimized based on the radiation patterns of the antenna were evaluated using an OMP algorithm. Furthermore, it was shown that once a target is detected, a circular polarization LOS communication link can be established to the detected target using a predefined polarization. The orthogonality of the polarizations allows the receiver to distinguish a received radar echo from an incident communications link. Furthermore, receive beamforming tailored to the M^{3}PA-element was shown to successfully suppress a strong incident communication link, when the time slot is supposed to be utilized for sensing rather than reception of the communication signal. Finally, the capacity of the polarization-based communication link employing circular beamforming was evaluated for different SNR and SIR constellations, showing that normalized capacities of 10 bps/Hz can be achieved, if the SIR is sufficiently high.

APPENDIX
A. DERIVATION OF THE ORTHODROME (SPHERICAL COORDINATES)

The shortest distance between two points on a sphere with angular coordinates (ϑ_1, φ_1) and (ϑ_2, φ_2) can be described by applying the scalar product according to

$$
\boldsymbol{r}_1^T\boldsymbol{r}_2 = r_1 r_2 \begin{bmatrix} \sin(\vartheta_1)\sin(\varphi_1) \\ \sin(\vartheta_1)\cos(\varphi_1) \\ \cos(\vartheta_1) \end{bmatrix}^T \begin{bmatrix} \sin(\vartheta_2)\sin(\varphi_2) \\ \sin(\vartheta_2)\cos(\varphi_2) \\ \cos(\vartheta_2) \end{bmatrix}
$$
$$
= |r_1||r_2|\cos(\xi). \tag{42}
$$

The angle ξ describes the opening angle between the two position vectors $\boldsymbol{r}_1$ and $\boldsymbol{r}_2$ in spherical coordinates. Given the same radius $r_1 = r_2 \in \mathbb{R}$, one obtains

$$\cos(\xi) = \sin(\vartheta_1)\sin(\vartheta_2)(\cos(\varphi_1)\cos(\varphi_2) + \sin(\varphi_1)\sin(\varphi_2))$$
$$+ \cos(\vartheta_1)\cos(\vartheta_2). \tag{43}$$

The application of the theorem

$$\cos(x \pm y) = \cos(x)\cos(y) \mp \sin(x)\sin(y) \tag{44}$$

results in

$$\cos(\xi) = \sin(\vartheta_1)\sin(\vartheta_2)\cos(\varphi_1 - \varphi_2)$$
$$+ \cos(\vartheta_1)\cos(\vartheta_2). \tag{45}$$

ACKNOWLEDGMENT

REFERENCES

[1] X. Fang, W. Feng, Y. Chen, N. Ge, and Y. Zhang, "Joint communication and sensing toward 6G: Models and potential of using MIMO," *IEEE Internet Things J.*, vol. 10, no. 5, pp. 4093–4116, Mar. 2023.

[2] J. Mietzner, "DFT-spread OFDM MIMO-radar—An alternative for reduced crest factors," in *Proc. 20th Int. Radar Symp. (IRS)*, Jun. 2019, pp. 1–10.

[3] M. Schurwanz, J. Mietzner, and P. A. Hoeher, "DFT-spread OFDM frequency domain processing for joint MIMO radar and communication," in *Proc. 26th Workshop Smart Antennas (WSA) 13th Conf. Syst. Commun. Coding (SCC)*, Feb. 2023, pp. 1–6.

[4] K. Wu, J. A. Zhang, X. Huang, and Y. J. Guo, "OTFS-based joint communication and sensing for future Industrial IoT," *IEEE Internet Things J.*, vol. 10, no. 3, pp. 1973–1989, Feb. 2023.

[5] F. Liu, C. Masouros, A. P. Petropulu, H. Griffiths, and L. Hanzo, "Joint radar and communication design: Applications, state-of-the-art, and the road ahead," *IEEE Trans. Commun.*, vol. 68, no. 6, pp. 3834–3862, Jun. 2020.

[6] Q. Wu et al., "A comprehensive overview on 5G-and-beyond networks with UAVs: From communications to sensing and intelligence," *IEEE J. Sel. Areas Commun.*, vol. 39, no. 10, pp. 2912–2945, Oct. 2021.

[7] G. Geraci et al., "What will the future of UAV cellular communications be? A flight from 5G to 6G," *IEEE Commun. Surveys Tuts.*, vol. 24, no. 3, pp. 1304–1335, 3rd Quart., 2022.

[8] D. Manteuffel and R. Martens, "Compact multimode multielement antenna for indoor UWB massive MIMO," *IEEE Trans. Antennas Propag.*, vol. 64, no. 7, pp. 2689–2697, Jul. 2016.

[9] N. Peitzmeier and D. Manteuffel, "Selective excitation of characteristic modes on an electrically large antenna for MIMO applications," in *Proc. Eur. Conf. Antennas Propag. (EuCAP)*, London, U.K., Apr. 2018, pp. 1–5.

[10] N. Peitzmeier and D. Manteuffel, "Upper bounds and design guidelines for realizing uncorrelated ports on multimode antennas based on symmetry analysis of characteristic modes," *IEEE Trans. Antennas Propag.*, vol. 67, no. 6, pp. 3902–3914, Jun. 2019.

[11] N. Peitzmeier and D. Manteuffel, "Multi-mode antenna concept based on symmetry analysis of characteristic modes," in *Proc. Eur. Conf. Antennas Propag. (EuCAP)*, Apr. 2019, pp. 1–5.

[12] T. Wu and F. H. Lin, "Multi-mode multi-port (M3P) Metaloop antenna for near-field sensing and communication using characteristic mode analysis," in *Proc. Int. Conf. Microw. Millimeter Wave Technol. (ICMMT)*, May 2023, pp. 1–3.

[13] G. Federico, Z. Song, G. Theis, D. Caratelli, and A. B. Smolders, "Multi-mode antennas for ultra-wide-angle scanning millimeter-wave arrays," *IEEE Open J. Antennas Propag.*, vol. 4, pp. 912–923, Aug. 2023.

[14] Z. Zhou, Z. Wei, Z. Tang, Y. Yin, and J. Ren, "Compact and Wideband differentially fed dual-Polarized antenna with high common-mode suppression," *IEEE Access*, vol. 7, pp. 108818–108826, 2019.

[15] L. Möerlein and D. Manteuffel, "Understanding single-element beamforming using characteristic modes and a change of basis," in *Proc. 16th Eur. Conf. Antennas Propagat. (EuCAP)*, May 2022, pp. 1–3.

[16] N. L. Johannsen, N. Peitzmeier, P. A. Hoeher, and D. Manteuffel, "On the feasibility of multi-mode antennas in UWB and IoT applications below 10 GHz," *IEEE Commun. Mag.*, vol. 58, no. 3, pp. 69–75, Mar. 2020.

[17] S. A. Almasri, R. Pöhlmann, N. Doose, P. A. Hoeher, and A. Dammann, "Modeling aspects of planar multi-mode antennas for direction-of-arrival estimation," *IEEE Sensors J.*, vol. 19, no. 12, pp. 4585–4597, Jun. 2019.

[18] R. Pöhlmann, S. Almasri, S. Zhang, T. Jost, A. Dammann, and P. Hoeher, "On the potential of multi-mode antennas for direction-of-arrival estimation," *IEEE Trans. Antennas Propag.*, vol. 67, no. 5, pp. 3374–3386, May 2019.

[19] A. Harlakin, J. Mietzner, P. A. Hoeher, and A. Meusling, "Compressive-sensing-aided MIMO radar enabling multi-functional and compact sensors in air scenarios using optimized antenna arrays," *IEEE Access*, vol. 9, pp. 41417–41429, 2021.

[20] X. Tong, Z. Zhang, J. Wang, C. Huang, and M. Debbah, "Joint multi-user communication and sensing exploiting both signal and environment sparsity," *IEEE J. Sel. Topics Signal Process.*, vol. 15, no. 6, pp. 1409–1422, Nov. 2021.

[21] K. Meng, Q. Wu, S. Ma, W. Chen, and T. Q. S. Quek, "UAV trajectory and Beamforming optimization for integrated periodic sensing and communication," *IEEE Wireless Commun. Lett.*, vol. 11, no. 6, pp. 1211–1215, Jun. 2022.

[22] Z. Gao et al., "Integrated sensing and communication with mmWave massive MIMO: A compressed sampling perspective," *IEEE Trans. Wireless Commun.*, vol. 22, no. 3, pp. 1745–1762, Mar. 2023.

[23] P. Kumari, N. J. Myers, and R. W. Heath, "Adaptive and fast combined waveform-beamforming design for MMWave automotive joint communication-radar," *IEEE J. Sel. Topics Signal Process.*, vol. 15, no. 4, pp. 996–1012, Jun. 2021.

[24] A. Santra, A. R. Ganis, J. Mietzner, and V. Ziegler, "Ambiguity function and imaging performance of coded FMCW waveforms with fast 4D receiver processing in MIMO radar," *Digit. Signal Process.*, vol. 97, Feb. 2020, Art. no. 102618. [Online]. Available: https://www.sciencedirect.com/science/article/pii/S1051200419301721

[25] W. M. Brown and R. J. Fredricks, "Range-doppler imaging with motion through resolution cells," *IEEE Aerosp. Electron. Syst. Mag.*, vol. AES-5, no. 1, pp. 98–102, Jan. 1969.

[26] N. L. Johannsen, S. A. Almasri, and P. A. Hoeher, "Geometry-based UAV MIMO channel modeling and pattern optimization for multimode antennas," *IEEE Trans. Antennas Propag.*, vol. 70, no. 11, pp. 11024–11032, Nov. 2022.

[27] N. L. Johannsen and P. A. Hoeher, "Single-element beamforming using multi-mode antenna patterns," *IEEE Wireless Commun. Lett.*, vol. 9, no. 7, pp. 1120–1123, Jul. 2020.